Electrochimica Acta 197 (2016) 330–335

Contents lists available at ScienceDirect

Electrochimica Acta

journal homepage: www.elsevier.com/locate/electacta

Analysis and Control of the Initial Electrodeposition Stages of Co-Pt Nanodot Arrays

Siggi Wodarz, Junya Abe, Takayuki Homma*

Department of Applied Chemistry, Waseda University, Shinjuku, Tokyo 169-8555, Japan

ARTICLE INFO

Article history:
Received 12 September 2015
Received in revised form 20 November 2015
Accepted 27 November 2015
Available online 30 November 2015

Keywords:
Electrodeposition
Initial deposition
Nanodot array
Bit-patterned media
CoPt alloy

ABSTRACT

We have fabricated Co-Pt nanodot arrays by combining electrodeposition with electron beam lithography (EBL) for applications in ultra-high density magnetic recording media, such as bit-patterned media (BPM). In this work, we analyzed the initial nucleation and growth of Co-Pt inside nanopores to achieve nanodot arrays with high deposition uniformity, as well as magnetic properties. At −900 mV (vs. Ag/AgCl), multiple nuclei of 2.0–3.0 nm in size were randomly distributed, even in nanopores with a 10 nm diameter, which could result in a lack of uniformity in the magnetic properties. The number of nuclei was then reduced by applying a less negative potential (>−700 mV vs. Ag/AgCl) to deposit a single nucleus inside each nanopore. As a result, a single grain of 5.0–10 nm in size was successfully deposited inside the nanopore, which could induce uniform magnetic properties in each nanodot. In addition, at less negative potentials, the coercivity of the Co-Pt films increased, which was induced by the epitaxial-like growth of Co-Pt from the Ru substrate. Cross-sectional TEM analysis suggested that Co-Pt deposited with a less negative potential was single crystalline with uniform hcp lattice fringes in the direction perpendicular to the Ru interface, indicating the formation of highly uniform nanodot arrays with high perpendicular magnetic anisotropy.

1. Introduction

As the amount of information continues to increase explosively, areal recording densities of hard disk drives, which play a major role in magnetic storage devices, are required to be on the order of Tbit/inch^2. To achieve ultra-high magnetic recording density, magnetic grain sizes have to be reduced to within several nanometers. However, reducing the grain size in conventional magnetic recording media has become increasingly difficult owing to the thermal instability (superparamagnetic limit) of small grain media, which results in loss of stored data and, furthermore, media noise caused by exchange coupling between adjacent magnetic grains. In order to solve these problems, energy assisted recording media [1,2] and bit-patterned media (BPM) [3,4] have been studied actively as candidates for the next generation of ultra-high density magnetic recording media. In BPM, the magnetic layer consists of arrayed ferromagnetic nanodots, in which magnetic grains are physically isolated; thus, interaction between each grain is negligible, which enables Tbit-level recording densities to be achieved. In such cases, a single magnetic domain structure is highly desirable owing to its low media noise and high coercivity, and thus it is essential to miniaturize the size of nanodot arrays while avoiding the superparamagnetic limit.

For application in BPM, nanodot arrays have been fabricated using several approaches, such as self-assembly of magnetic nanoparticles [5–7] and patterning of sputtered magnetic films by combining photolithography with a dry etching process [8–11]. However, the former approach faces the difficult challenge of controlling the crystal orientation of the magnetic particles, and in the latter approach, non-uniformity of the magnetic properties is caused by damage during the etching process. This lack of uniformity in the magnetic properties of each nanodot is a critical issue for achieving high recording performance in BPM with Tbit-level densities. On the other hand, because electrodeposition exhibits the excellent features of high controllability and deposition uniformity on the nanoscale, in principle, it is possible to deposit single grains with uniform magnetic properties in each nanopore.

Utilizing these features, we have fabricated nanodot arrays by combining the lithography technique with electrodeposition [12–14]. Co-Pt alloy film with about 20 at% Pt is known to possess high perpendicular magnetic anisotropy without an annealing treatment due to its hexagonal-closed-packed (hcp) structure [15–17], which makes it suitable for fundamental studies of nanodot arrays

* Corresponding author.
E-mail address: t.homma@waseda.jp (T. Homma).

http://dx.doi.org/10.1016/j.electacta.2015.11.136
0013-4686/

fabrication. In a previous study [18], we successfully fabricated Co-Pt nanodot arrays with recording densities of 1 Tbit/inch^2 by adapting electron beam lithography (EBL), which has high resolution capability and placement accuracy for fabrication of nanopore patterns [19,20], to demonstrate that electrochemical processes are suitable for BPM fabrication. At such ultra-high recording densities, the nanodots are miniaturized to 10 nm in diameter; therefore, to control the magnetic properties and deposition uniformity, it is essential to understand the mechanism of the initial stages of Co-Pt deposition inside the nanopore, especially to achieve fabrication of nanodot arrays consisting of single grains, which is highly desirable for application in BPM. Thus, in the present work, our objectives were to analyze the initial nucleation and growth processes of Co-Pt inside the nanopores under various conditions, such as different applied potentials and sizes of nanopores, to achieve precise control of the deposition.

2. Experimental

(002) oriented Ru (60 nm), which enhances the perpendicular magnetic anisotropy of Co-Pt [21,22], and Ti (5 nm) as an adhesion layer were sputter deposited onto an n-type Si (100) substrate. Prior to the nanopattern fabrication, the substrate surface was rinsed with acetone, ethanol, and ultra-pure water (UPW) for 5.0 min each. Then, an electron beam (EB) resist was coated onto the substrate at 5000 rpm to set the thickness of the layer at around 30 nm. For the EB resist, a mixture of positive-type EB resist (ZEP520A-7, Nippon Zeon) and diluent (ZEPA, Nippon Zeon) with a ratio of 1:2 was utilized. EBL was performed by using an EBL apparatus (ELS-7500, ELIONIX). After exposure, the substrate was developed by immersion in isopropanol for 5.0 s at 278 K and then rinsing with UPW. Prior to the Co-Pt electrodeposition, the substrate was exposed to excimer UV irradiation for 30 s to remove the residue at the bottom of the nanopores.

An electrolyte containing $Pt(NH_3)_2(NO_2)_2$ and 100 mmol L^{-1} of $CoSO_4$, $(NH_4)_2C_6H_6O_7$, and NH_2CH_2COOH was used [18,23]. The concentration of $Pt(NH_3)_2(NO_2)_2$ was adjusted for each deposition condition to maintain the film composition (Co:Pt = 80:20). The bath temperature was 303 K, and the bath pH was adjusted to 5.2 by adding NaOH. Electrodeposition of Co-Pt was performed under a constant applied potential using a potentiostat (HZ-5000, Hokuto Denko) with a three-electrode system consisting of Co wire as the counter electrode and a Ag/AgCl electrode as the reference electrode.

Magnetic characterization of the deposited films was carried out with polar optical Kerr effect equipment (BH-810CPC-WU, NEOARK). X-ray diffraction (XRD) patterns of the deposited films were collected using an X-ray diffractometer (Rint-UltimaIII, Rigaku) using CuK radiation (λ = 1.54184 Å). Morphological and structural characterizations of the electrodeposited Co-Pt nanodot arrays were performed using a high resolution scanning electron microscopy (HR-SEM, S5500, Hitachi High-Tech.) and transmitting electron microscopy (TEM, JEM$^-$2010, JEOL) after removing the entire EB resist by exposure to excimer UV irradiation for 2.0 min and rinsing with ethanol and UPW.

3. Results and Discussion

In order to analyze the initial deposition stages of Co-Pt inside the ultra-fine nanopores, the Co-Pt nucleation and growth processes were observed by SEM. Prior to Co-Pt electrodeposition, nanopatterned substrates with 25, 15, and 10 nm diameter nanopores were fabricated by EBL. Co-Pt was then deposited on the nanopatterned substrate with an applied potential of −900 mV (vs. Ag/AgCl). Fig. 1 shows SEM images of deposited Co-Pt nuclei inside nanopores with different diameters. The deposition duration was set to 2.0 s, which is appropriate for depositing Co-Pt as nuclei to obtain clear images by SEM. As these images were taken after removal of the entire EB resist, the Ru surface, which appears as dark contrast, is exposed and the Co-Pt nuclei, which appear as bright contrast, are centered in each image. In the initial stage, Co-Pt was nucleated as fine grains of 2.0–3.0 nm in diameter and was randomly distributed on the Ru surface at the bottom of the nanopores. It should be noted that Co-Pt nucleated from the outer side of the nanopore, as the current density varies between the outer and inner side of a nanopore and is expected to be higher at the outer side [24,25]. In larger nanopores, a distinct difference in the current density led to Co-Pt nucleation from the outer side of the nanopore. On the other hand, in the smaller nanopore with a 10 nm diameter, nucleation of Co-Pt is much less likely to be affected by the difference in current density. Moreover, in the case of smaller nanopore the nucleation of Co-Pt was inhibited by the nucleation exclusion zone, which surrounds the nuclei [26–28]. When a nucleus is formed on the surface, a zone of reduced concentration and overpotential is created around the nucleus that inhibits further nucleation. In the case of the nanopore with a 10 nm diameter, this inhibited zone may cover the bottom surface of the nanopore and influence the nucleation active site, resulting in a reduced number of nuclei. However, multinucleation of Co-Pt occurs even in the nanopore with a 10 nm diameter.

Fig. 2 shows SEM images of the growth of Co-Pt into 10 nm nanopore deposited with −900 mV (vs. Ag/AgCl) for 2.0, 3.0, and 5.0 s. As several nuclei of 2.0–3.0 nm in size were distributed on the bottom surface at an early stage, they grew as a cluster with several grain boundaries. This random and multinucleation could result in a lack of uniformity in the coercivity of each Co-Pt dot. Moreover, the superparamagnetic properties of Co-Pt particles should be considered, as this is a critical issue for BPM with Tbit-level densities. For application in the recording layer of a hard disk drive, the energy barrier of magnetic materials is required to obey the following equation for permanent recording, where K_u is the magnetic anisotropy constant, V is the volume of the particles, k_B is

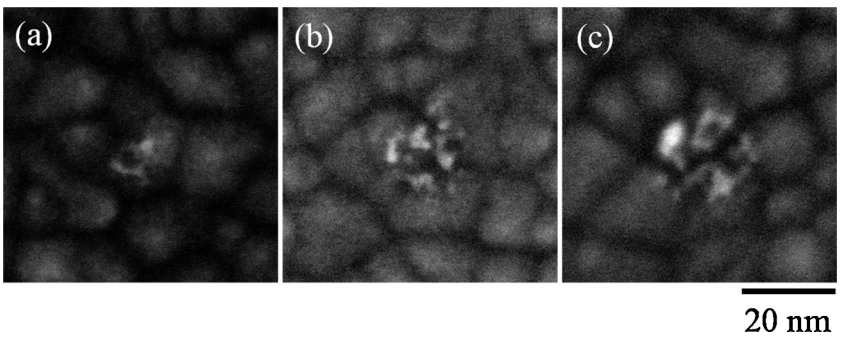

Fig. 1. SEM images of Co-Pt deposited with −900 mV (vs. Ag/AgCl) for 2.0 s in nanopore with different diameters: (a) 10 nm, (b) 15 nm, and (c) 25 nm.

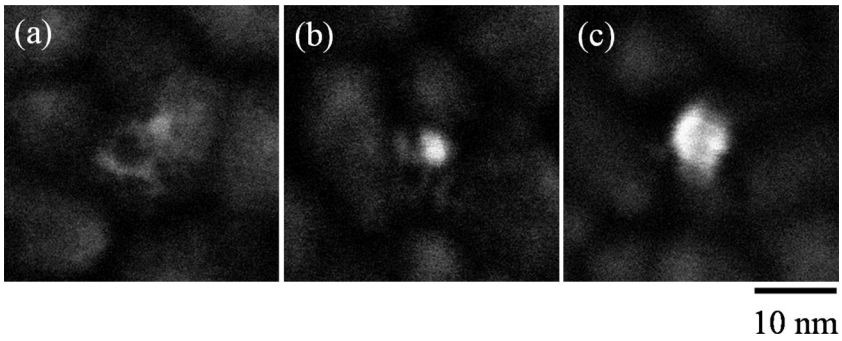

Fig. 2. SEM images of Co-Pt deposited with −900 mV (vs. Ag/AgCl) for (a) 2.0 s, (b) 3.0 s, and (c) 5.0 s inside nanopore with 10 nm diameter.

Boltzmann constant, and T is temperature.

$$K_u V > 60 k_B T \quad (1)$$

In Eq. (1), the superparamagnetic limit occurs when the product of K_u and V is less than the right-hand side; thus, it is possible to determine the critical size D_p from the volume when $K_u V$ equals $60\,k_B T$. If the Co-Pt nucleus is assumed to be a sphere, the critical particle diameter D_p is expressed by Eq. (2).

$$D_p = (60 \times 3/4\pi \times k_B T/K_u)^{1/3} \times 2 \quad (2)$$

The K_u value of hcp Co-Pt was 2.0×10^7 erg/cm^3 [15] and T was 298 K. According to Eq. (2), the critical size D_p was 6.2 nm. Based on this result, Co-Pt particles with a size of 2.0–3.0 nm are expected to be superparamagnetic. Therefore, to form Co-Pt dots with high coercivity, it is important to enhance the growth of Co-Pt by applying a less negative potential at which growth of the nucleus preferentially occurs to form larger size particles.

Hence, Co-Pt electrodeposition was carried out with an applied potential of −500 mV (vs. Ag/AgCl), which is within 100 mV of the reduction potential of Co-Pt so that slower growth can be achieved. SEM images were taken after deposition for 60 and 120 min in 25 nm nanopores, as shown in Fig. 3. The first image shows that the nucleation size of Co-Pt was 4.0–5.0 nm, which is larger than that observed in Fig. 1 or Fig. 2. After deposition for 120 min, the number of nuclei rarely differed from that at the early stage and the nuclei size increased to 5.0–7.0 nm. This reduction of nucleation density and increase of nucleus size were observed at potentials less negative than −700 mV (vs. Ag/AgCl) (data not shown). These results indicate that the growth of Co-Pt nuclei preferentially occurs over formation of a new nucleus, and thus a single nucleus should be grown in 10 nm nanopores using this potential range.

Because the deposition rate is extremely slow at −500 mV (vs. Ag/AgCl), which could cause the formation of non-uniform nanodot arrays, potential of −700 mV (vs. Ag/AgCl) was applied to deposit a single nucleus of Co-Pt in 10 nm nanopores. The composition of Co-Pt changes with applied potential, therefore in order to deposit a single Co-Pt nucleus concentration of Pt electrolyte is optimized in each applied potential condition to set the composition of Co-Pt alloy close to Co:Pt = 80:20. The composition of Pt is tend to increase at less negative potential, thus concentration of Pt electrolyte is reduced to 2.1 mM for −700 mV (vs. Ag/AgCl) compared with the concentration (2.4–3.0 mM) of −900 mV (vs. Ag/AgCl). The deposition duration was set to 30 min. As shown in Fig. 4, a single nucleus of Co-Pt was formed inside the nanopore that grew to a diameter of 5.0 nm at −700 mV (vs. Ag/AgCl) without any grain boundaries. Moreover, the nucleus grew in a columnar structure in the direction normal to the surface, which could improve the perpendicular magnetic anisotropy of nanodot arrays. These results suggested the successful formation of nanodot arrays with a single crystal structure by adjusting the applied potential to control the number and size of Co-Pt nuclei. The magnetic anisotropy and magnetic domain structure are sensitive to slight changes in crystal structure; thus, the coercivity of nanodot arrays should be strongly influenced by the potential, as a difference in crystal structure with potential was suggested.To investigate the effect of the applied potential on the magnetic properties, we characterized the hysteresis loops of Co-Pt films deposited with −700 and −900 mV (vs. Ag/AgCl) with thicknesses of 16 and 17 nm, respectively. Fig. 5 shows the hysteresis loops of each Co-Pt film, and composition, coercivity, and squareness of the Co-Pt continuous films are summarized in Table 1. The concentration of Pt

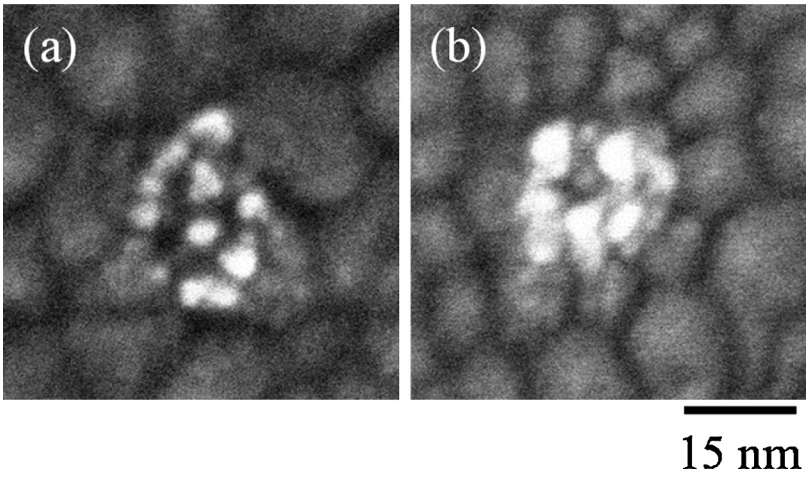

Fig. 3. SEM images of Co-Pt deposited with −500 mV (vs. Ag/AgCl) for (a) 60 min and (b) 120 min inside nanopore with 25 nm diameter.

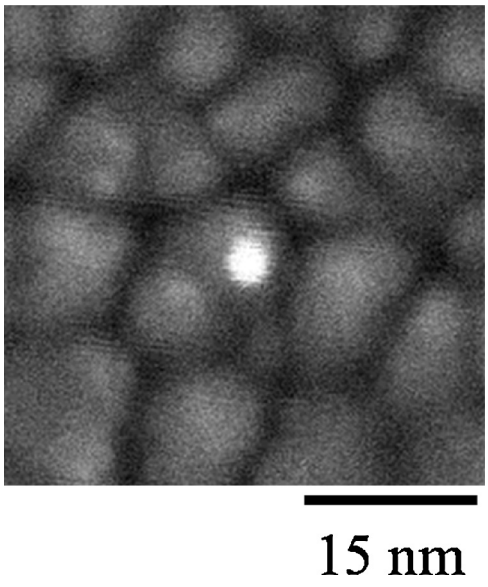

Fig. 4. SEM images of Co-Pt deposited with −700 mV (vs. Ag/AgCl) for 30 min inside nanopore with 10 nm diameter.

$(NH_3)_2(NO_2)_2$ was 2.1 and 3.0 mmol L^{-1} for −700 and −900 mV (vs. Ag/AgCl), respectively. As shown in Fig. 5, the coercivity of the Co-Pt film obtained using −700 mV (vs. Ag/AgCl) was higher than that of the film obtained using −900 mV (vs. Ag/AgCl), even though this film had a larger deviation from the ideal composition of Co:Pt = 80:20. The composition of the films were Co:Pt = 70:30 and 79:21 with −700 and −900 mV (vs. Ag/AgCl), respectively.

To evaluate the change in coercivity with potential, we analyzed the crystal structure of the Co-Pt films, as shown in Fig. 6. The XRD patterns of the Co-Pt films showed that, in the case of −700 mV (vs. Ag/AgCl), the peak corresponding to Co-Pt hcp (002), which appears at ~43.5°, is shifted to ~42.7° to overlap the peak of Ru hcp (002). The main reason for this shift is the change in the composition of the film. In substitutional solid solutions, such as Co-Pt, it is known that the lattice constant changes with respect to the composition of the alloy in accordance with Vegard's law. Thus, when the composition of Pt, which has a larger atomic radius than Co, increases, the lattice spacing of Co-Pt increases, resulting in a lower 2θ value. In order to investigate the peak shift, the 2θ value for each composition was calculated according to Vegard's law. The lattice constant a is expressed by Eq. (3).

$$a = \frac{2r_{Co}x + 2r_{Pt}(100 - x)}{100} \tag{3}$$

Table 1
Composition, coercivity, and squareness of Co-Pt continuous film.

Applied potential/mV	Composition (at%)	Coercivity /kOe	Squareness
−900	$Co_{79}Pt_{21}$	1.3	0.28
−700	$Co_{70}Pt_{30}$	1.7	0.30

where r_{Co} is the atomic radius of Co (125 pm), r_{Pt} is the atomic radius of Pt (139 pm), and x is the composition of Co (%). The relation between the lattice constant and lattice spacing is expressed by Eq. (4).

$$\frac{1}{d^2} = \frac{4}{3}\left(\frac{h^2 + hk + k^2}{a^2}\right) + \frac{l^2}{c^2} \tag{4}$$

In the case of hcp (002), the (h,k,l) value is (002), and thus the lattice spacing c is described as $c = 2d$. As the ratio of the lattice constants a and c for Co is known to be $c = 1.6237a$, we assumed that Co-Pt has the same ratio. Based on these equations, the lattice spacing d was calculated, and 2θ was obtained from the Bragg equation, where n is an integer and λ is the wavelength of the incident wave (1.54178 Å for CuKα).

$$d = \frac{n\lambda}{2\sin\theta} \tag{5}$$

The 2θ values calculated from the composition of each film were 43.5° (Co:Pt = 79:21) for −900 mV (vs. Ag/AgCl) and 43.0° (Co:Pt = 70:30) for −700 mV (vs. Ag/AgCl). In the case of −900 mV (vs. Ag/AgCl), the calculated angle was the same as that observed in the XRD pattern. On the other hand, in the case of −700 mV (vs. Ag/AgCl), because the peak in the pattern is shifted to a lower angle than that calculated using Vegard's law, a further increase in the lattice spacing was suggested. This indicates that Co-Pt has grown along the Ru crystal orientation, which has slightly larger lattice spacing than Co-Pt, to broaden its lattice spacing. This epitaxial-like growth could enhance the perpendicular magnetic anisotropy and increase the coercivity of the film deposited with −700 mV (vs. Ag/AgCl).

Considering the growth conditions of Co-Pt films deposited with a less negative potential, in nanodot arrays, as Co-Pt is not only grown along the Ru surface but is also deposited as a single nucleus, the coercivity should be improved with the less negative potential. Fig. 7 shows cross-sectional TEM images of Co-Pt deposited with −900, −700, and −600 mV (vs. Ag/AgCl) inside 10 nm nanopores. To confirm the above assumption, we observed the growth conditions of Co-Pt inside nanopores using TEM. In Fig. 7(a) and (b), the thickness of the EB resist was reduced from 30 to 20 nm by the excimer-UV pretreatment, and mushroom-shaped nanodot arrays were observed owing to overfilling of Co-Pt.

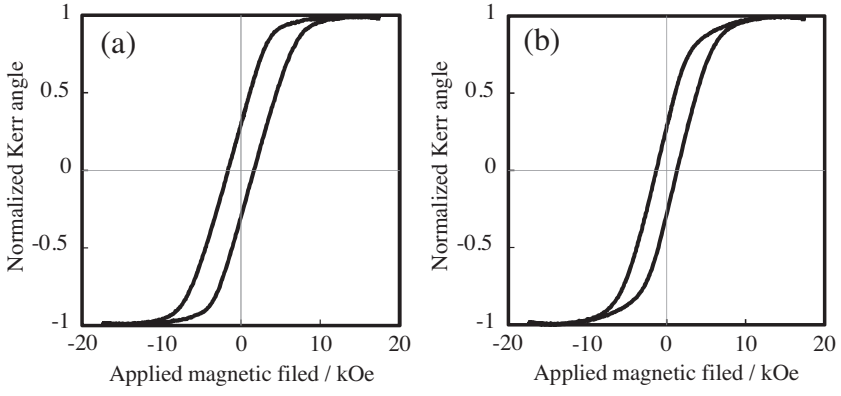

Fig. 5. Hysteresis loops of Co-Pt films deposited with (a) −700 mV (vs. Ag/AgCl) and (b) −900 mV (vs. Ag/AgCl). Thickness of the films is (a) 16 nm and (b) 17 nm, respectively.

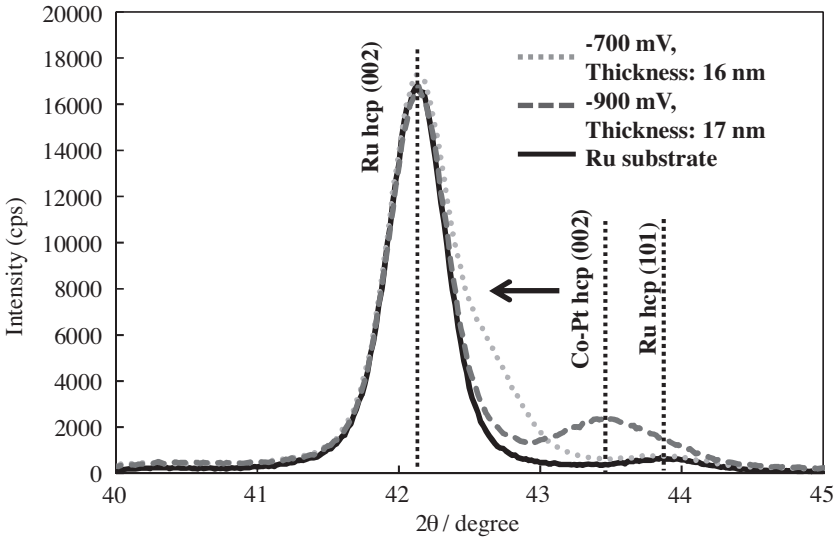

Fig. 6. XRD spectra of Co-Pt films deposited with −700 mV and −900 mV (vs. Ag/AgCl) and Ru substrate.

In this overfilled region, a polycrystalline structure with fine grain structure was confirmed, which may be due to hemispherical diffusion of metal ions to expand the Co-Pt nucleation site. Nevertheless, columnar structures of nanodot arrays without voids were observed inside the nanopore. Figs. 7(d), (f), and (h) show high magnification TEM images of the interface between Co-Pt and Ru, and the insets show the electron beam diffraction of each nanodot. In these images, lattice fringes in the direction perpendicular to the Ru interface were observed. Furthermore, the diffraction images showed rings and spots corresponding to hcp (002), indicating that Co-Pt grew along the Ru crystal orientation with high crystallinity in the initial deposition stage, which is expected to induce perpendicular magnetic anisotropy in the nanodot arrays. In addition, from the diffraction images, diffraction rings and diffraction spots that correspond to polycrystalline and single crystalline structures were observed for -900 mV (vs. Ag/AgCl) and the less negative potentials of −700 mV and −600 mV (vs. Ag/AgCl), respectively, indicating different Co-Pt growth conditions for −900 mV (vs. Ag/AgCl) and the less negative potentials. Figs. 7(g) and (h) show higher magnification TEM images of the upper part of the Co-Pt nanodot. In Fig. 7(g), the Co-Pt lattice is randomly oriented, suggesting that multinucleation, including secondary nucleation, occurs to form grain boundaries at −900 mV (vs. Ag/AgCl), which resulted in a nanodot with a polycrystalline structure. On the other hand, in Fig. 7(f) and (h), clear stacking of hcp lattices without any grain boundaries was

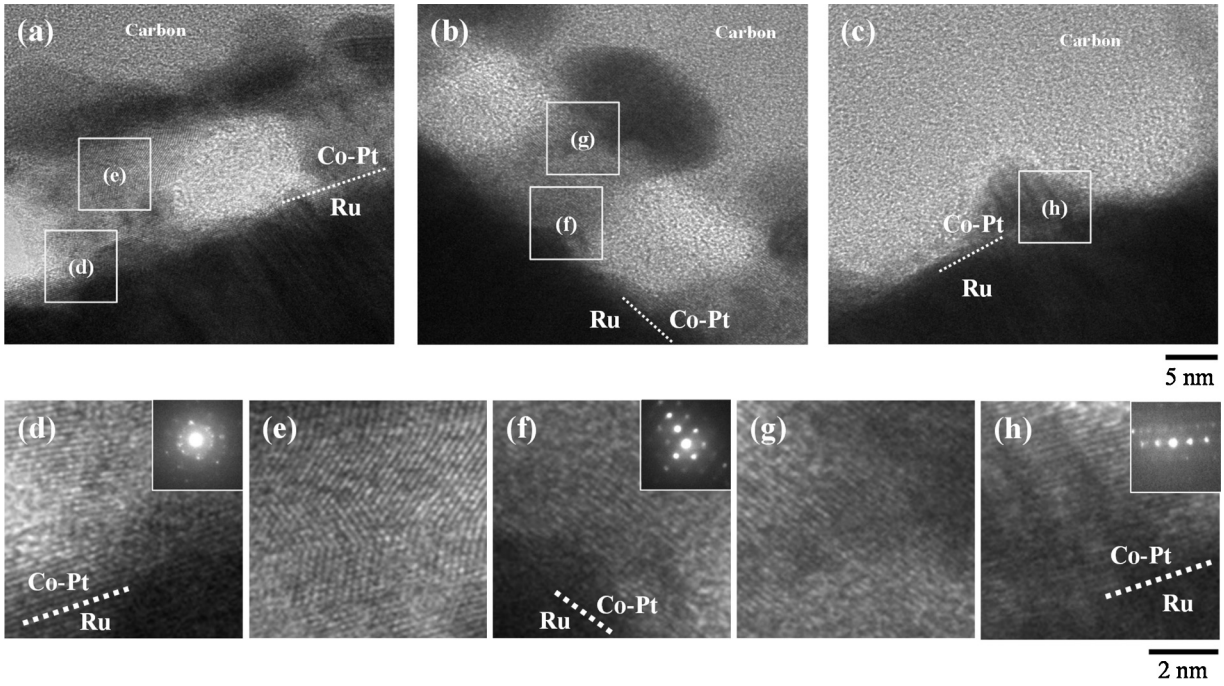

Fig. 7. Cross-sectional TEM images of Co-Pt nanodot arrays with 10 nm diameter and 35 nm pitch deposited with (a) −900 mV, (b) −700 mV, and (c) −600 mV (vs. Ag/AgCl). High magnification images at (d, f, h) interface of Co-Pt and Ru substrate and (e, g) upper part of Co-Pt nanodot arrays. The insets show the electron beam diffraction of nanodot arrays deposited with each potential.

observed, even in the upper section of the nanodot. These results indicated that, with a less negative potential, a single nucleus of Co-Pt was formed inside the nanopore that subsequently grew from the interface of Ru in a perpendicular orientation to form a single crystalline structure.

Based on the above results, by controlling the nucleation and growth behavior of Co-Pt, our attempts to fabricate single crystal Co-Pt nanodot arrays were successful. To achieve further precise control of the initial deposition stage, the nucleation density and kinetic behavior inside the nanopores should be examined in more detail in future studies.

4. Conclusion

In the present work, we analyzed the initial electrodeposition stages of Co-Pt inside ultra-fine nanopores to fabricate Co-Pt nanodot arrays with a single crystalline structure. At −900 mV (vs. Ag/AgCl), the number of nuclei decreased in smaller nanopores, but multinucleation was observed, even in 10 nm nanopores. On the other hand, at more less negative potentials (>−700 mV vs. Ag/AgCl), growth of the nucleus is preferential, and a single nucleus was formed inside the 10 nm nanopore that grew to form a columnar-structured grain with a size of 7.0–10 nm. In addition, at less negative potentials, Co-Pt grew along the Ru crystal orientation during the initial deposition stage to increase the coercivity of the Co-Pt films. Cross-sectional TEM images confirmed that, at less negative potentials, Co-Pt grew as a single crystal with clear stacking of hcp lattices in the direction perpendicular to the interface of Ru. To achieve further deposition uniformity, it is important to analyze the initial nucleation and growth stages of Co-Pt in more detail.

Acknowledgements

This work was supported in part by JSPS KAKENHI Grant Number 25249104.

References

[1] M.H. Kryder, E.C. Gage, T.W. McDaniel, W.A. Challener, R.E. Rottmayer, G. Ju, Y.T. Hsia, M.F. Erden, Heat assisted magnetic recording, Proc. IEEE 96 (2008) 1810.
[2] Y. Shiroishi, K. Fukuda, I. Tagawa, H. Iwasaki, S. Takenoiri, H. Tanaka, H. Mutoh, N. Yoshikawa, Future options for HDD storage, IEEE Trans. Magn. 45 (2009) 3816.
[3] H.J. Richter, A.Y. Dobin, O. Heinonen, K.Z. Gao, R.J.M.v.d. Veerdonk, R.T. Lynch, J. Xue, D. Weller, P. Asselin, M.F. Erden, R.M. Brockie, Recording on bit-patterned media at densities of 1 Tb/in^2 and beyond, IEEE, Trans Magn. 42 (2006) 2255.
[4] J.C. Lodder, Methods for preparing patterned media for high-density recording, J. Magn. Magn. Mater. 272–276 (2004) 1692.
[5] B.D. Terris, T. Thomson, Nanofabricated and self-assembled magnetic structures as data storage media, J. Phys. D: Appl. Phys. 38 (2005) R199.
[6] T. Hachisu, W. Sato, S. Ishizuka, A. Sugiyama, J. Mizuno, T. Osaka, Injection of synthesized FePt nanoparticles in hole-patterns for bit patterned media, J. Magn. Magn. Mater. 324 (2012) 303.
[7] S. Sun, C.B. Murray, D. Weller, L. Folks, A. Moser, Monodisperse FePt nanoparticles and ferromagnetic FePt nanocrystal superlattices, Science 287 (2000) 1989.
[8] B.D. Terris, Fabrication challenges for patterned recording media, J. Magn. Magn. Mater. 321 (2009) 512.
[9] G.M. McClelland, M.W. Hart, C.T. Rettner, M.E. Best, K.R. Carter, B.D. Terris, Nanoscale patterning of magnetic islands by imprint lithography using a flexible mold, Appl. Phys. Lett. 81 (2002) 1483.
[10] J.Y. Cheng, C.A. Ross, V.Z.H. Chan, E.L. Thomas, R.G.H. Lammertink, G.J. Vancso, Formation of a cobalt magnetic dot array via block copolymer lithography, Adv. Mater. 13 (2001) 1174.
[11] O. Hellwig, J.K. Bosworth, E. Dobisz, D. Kercher, T. Hauet, G. Zeltzer, J.D. Risner-Jamtgaard, D. Yaney, R. Ruiz, Bit patterned media based on block copolymer directed assembly with narrow magnetic switching field distribution, Appl. Phys. Lett. 96 (2010) 052511.
[12] T. Ouchi, Y. Arikawa, T. Kuno, J. Mizuno, S. Shoji, T. Homma, Electrochemical fabrication and characterization of CoPt bit patterned media: Towards a wetchemical, large-scale fabrication, IEEE Trans. Magn. 46 (2010) 2224.
[13] T. Ouchi, Y. Arikawa, T. Homma, Fabrication of CoPt magnetic nanodot arrays by electrodeposition process, J. Magn. Magn. Mater. 320 (2008) 3104.
[14] T. Ouchi, Y. Arikawa, Y. Konishi, T. Homma, Fabrication of magnetic nanodot array using electrochemical deposition processes, Electrochim. Acta 55 (2010) 8081.
[15] D. Weller, A. Moser, L. Folks, M.E. Best, W. Lee, M.F. Toney, M. Schwickert, J.U. Thiele, M.F. Doerner, High K_u materials approach to 100 Gbits/in^2, IEEE Trans. Magn. 36 (2000) 10.
[16] I. Zana, G. Zangari, M. Shamsuzzoha, Enhancing the perpendicular magnetic anisotropy of Co–Pt(P) films by epitaxial electrodeposition onto Cu(1 1 1) substrates, J. Magn. Magn. Mater. 292 (2005) 266.
[17] G. Pattanaik, J. Weston, G. Zangari, Magnetic properties of Co-rich Co–Pt thin films electrodeposited on a Ru underlayer, J. Appl. Phys. 99 (2006) 08E901.
[18] T. Homma, S. Wodarz, D. Nishiie, T. Otani, S. Ge, G. Zangari, Fabrication of FePt and CoPt magnetic nanodot arrays by electrodeposition process, Electrochem. Soc. Trans. 64 (2015) 1.
[19] X.M. Yang, S. Xiao, W. Wu, Y. Xu, K. Mountfield, R. Rottmayer, K. Lee, D. Kuo, D. Weller, Challenges in 1 Teradot/in.^{2} dot patterning using electron beam lithography for bit-patterned media, J. Vac. Sci. Technol. B 25 (2007) 2202.
[20] X.M. Yang, L. Wan, S. Xiao, Y. Xu, D.K. Weller, Directed block copolymer assembly versus electron beam lithography for bit-patterned media with areal density of 1 Terabit/inch^2 and beyond, ACS Nano 3 (2009) 1844.
[21] S.N. Piramanayagam, K. Srinivasan, Recording media research for future hard disk drives, J. Magn. Magn. Mater. 321 (2009) 485.
[22] G.H. Jeong, C.H. Lee, J.H. Jang, N.J. Park, S.J. Suh, The microstructure and magnetic properties of electrodeposited Co–Pt thin films on Ru buffer layer, J. Magn. Magn. Mater. 320 (2008) 2985.
[23] I. Zana, G. Zangari, Electrodeposition of Co-Pt films with high perpendicular anisotropy, Solid-State Lett 6 (2003) C153.
[24] L.T. Romankiw, A path: From electroplating through lithographic masks in electronics to LIGA in MEMS, Electrochim. Acta 12 (1997) 2985.
[25] S. Wodarz, T. Otani, H. Hagiwara, T. Homma, Characterization of electrodeposited Co-Pt nanodot array at initial deposition stage, Electrochem. Soc. Trans. 64 (2015) 99.
[26] B.R. Scharifker, G. Hills, Theoretical and experimental studies of multiple nucleation, Electrochim. Acta 28 (1983) 879.
[27] B.R. Scharifker, J. Mostany, Three-dimensional nucleation with diffusion controlled growth: Part I. Number density of active sites and nucleation rates per site, J. Electroanal. Chem. 177 (1984) 13.
[28] J. Ustarroz, X. Ke, A. Hubin, S. Bals, H. Terryn, New insights into the early stages of nanoparticle electrodeposition, J. Phys. Chem. C 116 (2012) 2322.